Environmental Science & Technology

Article

Cite This: Environ. Sci. Technol. 2019, 53, 7683−7693

pubs.acs.org/est

Effects of the Chemical Structure, Surface, and Micropore Properties of Activated and Oxidized Black Carbon on the Sorption and Desorption of Phenanthrene

Shujie Hu,[†,‡] Dainan Zhang,[†] Yu Yang,[†] Yong Ran,[*,†] Jingdong Mao,[§] Wenying Chu,[§] and Xiaoyan Cao[∥]

[†]State Key Laboratory of Organic Geochemistry, Guangzhou Institute of Geochemistry, Chinese Academy of Sciences, Guangzhou 510640, China

[‡]University of Chinese Academy of Science, Beijing 100049, China

[§]Department of Chemistry and Biochemistry, Old Dominion University, Norfolk, Virginia 23529, United States

[∥]Department of Chemistry, Brandeis University, Waltham, Massachusetts 02453, United States

Supporting Information

ABSTRACT: The effects of the chemical structure, surface properties, and micropore of modified black carbon samples (BCs) on the sorption mechanism of hydrophobic organic contaminants (HOCs) are discussed. Activated and oxidized BCs were produced from a shale kerogen at 250−500 °C by chemical activation regents (KOH and $ZnCl_2$) and then by oxidative regents (H_2O_2 and NaClO). The surface properties (water contact angel, Boehm titration, and cation exchange capacity, CEC), structural properties (advanced solid-state ^{13}C NMR), micropore properties (CO_2 adsorption), mesopore properties (N_2 adsorption), and sorption and desorption properties of phenanthrene were obtained. The results showed that $ZnCl_2$-activated BCs had higher basic surface groups, CEC values, aromatic carbon contents, micropore volumes, and adsorption volumes but exhibited lower acidic surface groups than the KOH-activated BCs did. Micropore modeling and sorption irreversibility indicated that the micropore filling was the main sorption mechanism of phenanthrene. In addition, $ZnCl_2$ activated and NaClO oxidized BCs showed a nice regression equation between adsorption volumes and micropore volumes (CO_2−V_0) as follows: $Q_0' = 0.495V_0 + 6.28 (R^2 = 0.98, p < 0.001)$. Moreover, the contents of nonprotonated aromatic carbon, micropore volumes, and micropore sizes are the critical factors to micropore filling mechanism of phenanthrene on BCs. The size of fused aromatic rings was estimated from the recoupled ^1H−^{13}C dipolar dephasing, and the BC structural models at temperatures ranging from 300 to 500 were proposed. This finding improves our understanding of the sorption mechanism of HOCs from the perspectives of chemical structure and micropore properties.

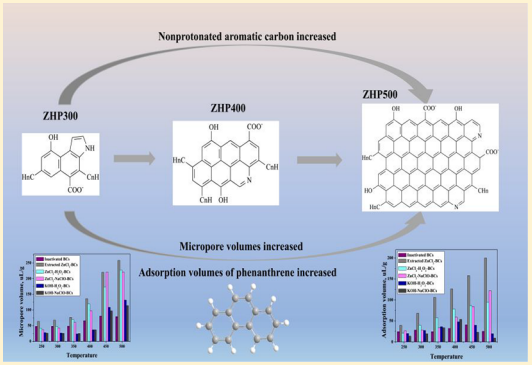

INTRODUCTION

Recently, black carbon samples (BCs) have received extensive attention due to their potential application for improving soil fertility, sequestering carbon, and feasible low-cost adsorbents to control the migration of contaminants.[1,2] In addition, some researchers have chemically modified black carbon to change its chemical properties and structural characteristics and to investigate its sorption mechanism. The sorption of hydrophobic organic contaminants (HOCs) on BCs is much higher than that on natural organic matter (NOM).[3] Many investigators have shown that the sorption mechanisms of HOCs on BCs are diverse, including specific sorption, nonspecific sorption, partitioning, and pore-filling.[4−7] Among them, the micropore-filling mechanism has been investigated in recent years. A few of the findings regarding the micropore-filling sorption mechanism of HOCs have been documented.[8,9] For example, Ran et al.[7] reported that micropore-filling of HOCs accounted for 45−98% of total sorption by peat and soil, and Zhang et al.[10] noted that 36−65% of HOCs can be adsorbed on kerogen by micropore-filling. Other investigations revealed that for condensed carbonaceous materials, organic carbon (OC) was the main medium to produce micropores, as significantly positive correlations were reported between the micropore volumes and OC contents or structure.[6,8,11] For example, it was found that the aliphatic C of the OC fractions and the aromatic C of biochars were key components determining their micropore and sorption behaviors of

Received: March 25, 2019
Revised: May 21, 2019
Accepted: June 7, 2019
Published: June 7, 2019

DOI: 10.1021/acs.est.9b01788
Environ. Sci. Technol. 2019, 53, 7683−7693

HOCs.[6] Duan et al.[11] demonstrated the important roles of aromatic carbon in the micropore and sorption behaviors of HOCs on thermally simulated kerogen. However, knowledge on the detailed chemical structures of the BCs and their micropore volumes and the sorption/desorption behaviors of the HOCs remain insufficient. The sorption mechanism on BCs requires further investigation. Moreover, the effects of micropore sizes of BCs on the sorption mechanisms of HOCs also need further investigation.

Chemical activation mainly focuses on a series of sorbents with excellent sorption capacity and with a given amount of functional −OH and −COOH groups.[8] Then, the structure and micropore properties of the samples are related to the sorption mechanism of the HOCs. Recently, activation has been widely used to regulate the micropore structures of carbon-rich materials.[12,13] Among the chemical activation agents, KOH and $ZnCl_2$ have mostly been used since they result in high micropore volumes.[13−17] The mechanism of $ZnCl_2$ activation is its dehydration during pyrolysis.[16] Moreover, $ZnCl_2$ can inhibit the carbon strcture contraction and promote the carbonization and aromatization of the carbon skeleton, thus promoting the development of micropore structures.[16,18] For KOH, the activation mechanism of carbonaceous materials can be explained by the combination of chemical activation, physical activation, and potassium insertion.[13] There are many reports on the preparation of activated carbon using $ZnCl_2$ and KOH, but few studies compare the difference of activated BCs in surface properties, chemical structural properties, and sorption properties of HOCs.[19−22]

The oxidation treatment can introduce oxygen-containing functional groups such as C═O, OH, and COOH, which are important to improve the cation exchange capacity and hydrophilicity of the BCs and to facilitate their dispersion in the aqueous phase.[8] In order to study the effect of microporous and surface properties on adsorption/desorption mechanism of HOCs on BCs, we combined activated and oxidized treatments to prepare BCs with improved micropores and surface oxygen functional groups; these treatments have rarely been conducted in earlier investigations. Specially, activated and oxidized BCs were first produced from a shale kerogen at temperatures ranging from 250 to 500 °C by chemical activation regents (KOH, $ZnCl_2$) and then were treated by oxidative regents (H_2O_2, NaClO). The objectives of this investigation were (1) to study and compare the surface properties, cation exchange capacities, micropore and mesopore properties, and structure properties of the different activated and oxidized BCs and (2) to examine the sorption/desorption isotherms and mechanism of phenanthrene on different activated and oxidized BCs, as well as (3) to explore the effect of micropore properties on sorption irreversibility of phenanthrene on BCs.

MATERIALS AND METHODS

Sample Collection and Treatments. Since the kerogen produces carbon-rich substances by pyrolysis, we chose kerogen as the raw material. The kerogen was produced by demineralization of an oil shale, which was collected from Maoming City and named as OS. The demineralization process has been described in other reports.[10,23] The $ZnCl_2$-activated and KOH-activated BCs were obtained by impregnation with $ZnCl_2$ or KOH, followed by slow pyrolysis under oxygen-limited conditions as previously reported.[10,14,24−29] The detailed descriptions are presented in the Supporting Information (SI). The $ZnCl_2$-activated black carbon samples (Z-BCs) produced at temperatures from 250 to 500 °C were named as Z250, Z300, Z350, Z400, Z450, and Z500. A portion of each of Z-BCs was extracted by dichloromethane and methanol to remove extractable organic matter (bitumen and tar, etc.). The extracted Z-BCs were named as E-Z-BCs, and then used in sorption and desorption experiments.

The H_2O_2 and NaClO treatments were based on earlier studies,[30,31] and the procedures can be found in one paper of our group.[8] The $ZnCl_2$-activated and H_2O_2-oxidized black carbon samples were named as ZHP-BCs. The $ZnCl_2$-activated and NaClO-oxidized samples were named as ZSH-BCs. Likewise, the KOH-activated and oxidized samples were named as PHP-BCs and PSH-BCs, respectively.

Characterization of the Activated and Oxidized BCs. The C, H, and N contents of the samples were measured using a Vario EL CUBE elemental analyzer (Elementar, Germany), and the O contents were measured with a Vario ELIII elemental analyzer (Elementar, Germany). The surface amphoteric properties of the samples were evaluated by Boehm titration.[32−34] The cation exchange capacities (CEC) of the samples were determined by the $BaCl_2$−H_2SO_4 method.[8] The water contact angle was measured by using a Contact Angel System OCA (Germany).[35] The chemical structures of the BCs were determined by multiple cross-polarization (multiCP) ^{13}CNMR.[36] The NMR experiments were performed on a Bruker Avance 400 spectrometer (Bruker, Billerica, MA) at 100 MHz for ^{13}C with a 4 mm double-resonance MAS probe head at a spinning of 14 kHz, with a 90° pulse-length of 4.2 μs for ^{1}H and 4 μs for ^{13}C.[36] The corresponding multiCP spectra of nonprotonated C and mobile C were obtained by combining the multiCP sequence with 68 μs recoupled dipolar dephasing (multiCP/DD).The different functional group assignments are as follows: 0−62 ppm, alkyl C; 62−92 ppm, O-alkyl C; 92−150 ppm, aromatic C (including aromatic C−C and aromatic C−H); 150−165 ppm, aromatic C−O; 165−190 ppm, COO; and 190−220 ppm, ketone/aldehyde.[11,37] The size of fused aromatic rings was estimated from the recoupled ^{1}H−^{13}C dipolar dephasing.[38,39] The CO_2 and N_2 isotherms were measured at 273 K and 77 K, respectively, by using a Micromeritics ASAP 2460 surface area and pore size analyzer. The surface areas (CO_2−SSA) and micropore volumes (CO_2−V_0) were calculated using the Dubinin-Radushkavich (*DR*) model,[9] and the micropore size distributions were estimated with density functional theory (DFT). The micropore and mesopore volumes of N_2 adsorption were measured by the *DR* model and Barrette-Joynere-Halenda (BJH) model, respectively.[24]

Batch Sorption and Desorption Experiments. Phenanthrene (>98%) was purchased from Aldrich Chemical Co. The solubility of phenanthrene in water is 1.12 mg/L, and the logK_{OW} is 4.57. The background solution (pH 7) contained 0.01 mol/L $CaCl_2$, 200 mg/L NaN_3, and 5 mg/L $NaHCO_3$. All sorption isotherms were obtained using a given amount of sorbent (0.1−1.23 mg) and a batch equilibration technique in 50 or 20 mL glass ampules at 25 ± 1 °C, 125 rpm. Batch phenanthrene sorption by the activated and oxidized BCs was performed as other investigations did, and described in the SI.[5,8]

Desorption experiments were investigated for the E-Z-BCs using flame-sealed glass ampules as batch reactors. Laboratory

DOI: 10.1021/acs.est.9b01788
Environ. Sci. Technol. 2019, 53, 7683−7693

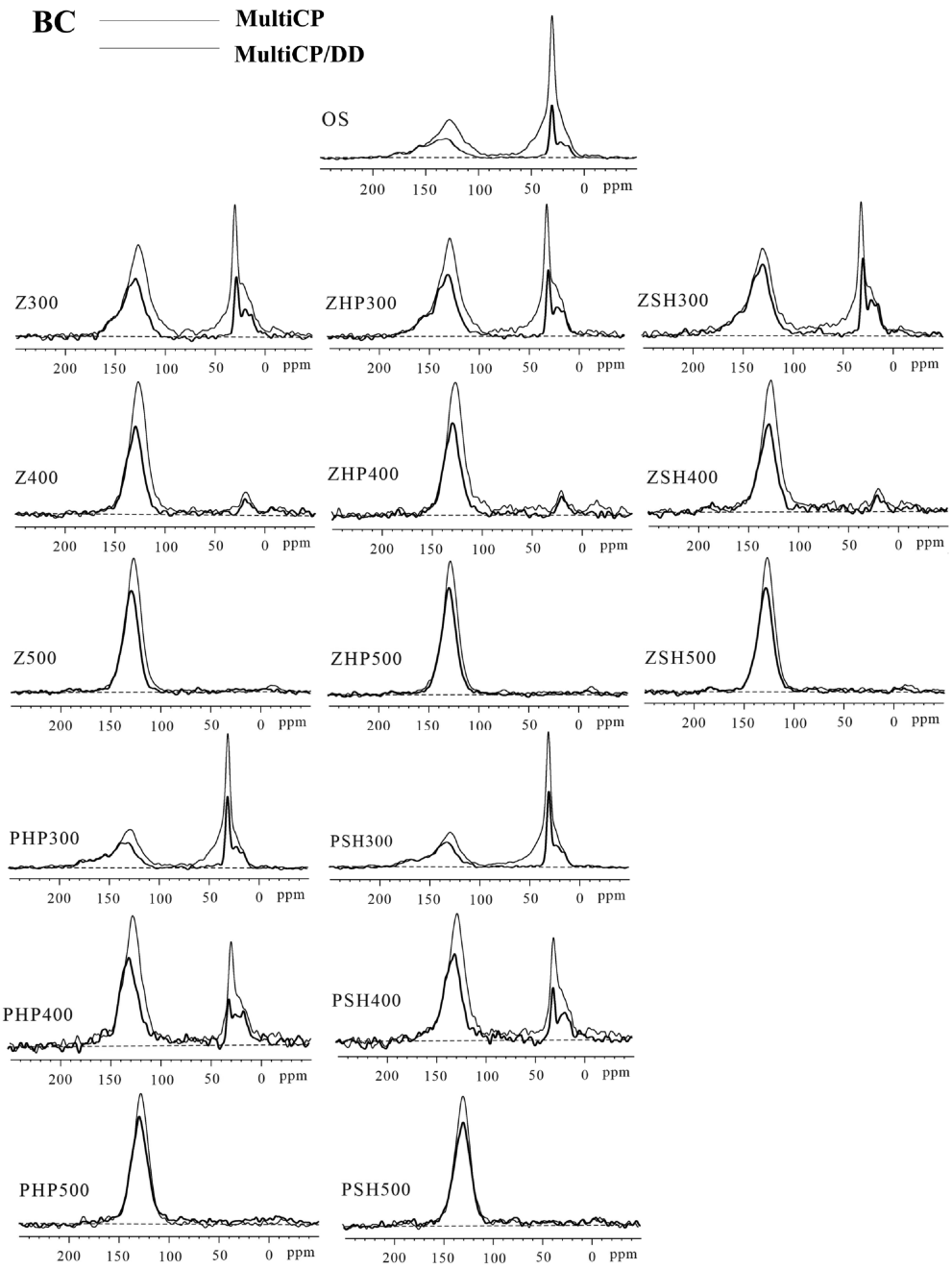

Figure 1. MultiCP/MAS spectra (thin lines) and multiCP/MAS ^{13}C NMR spectra after recoupled dipolar dephasing (thick lines) of the BCs.

procedures published elsewhere were followed exactly and presented in the SI.[40,41]

Sorption/Desorption Models. The Freundlich model (FM) is the most common model for describing the sorption/desorption of HOCs by heterogeneous adsorbents.[5,23] In addition, the Dubinin−Radushkevich (*DR*) model has been employed to describe the sorption isotherms from aqueous solutions onto micropore solids.[7,42] These models are listed in the SI.

RESULTS AND DISCUSSION

Compositions and Elemental Ratios of BCs. The OC contents of Z-BCs, E-Z-BCs, ZHP-BCs, and ZSH-BCs ranged from 71.2% to 76.0%, from 66.9% to 74.8%, from 68.4% to 73.0%, and from 62.9% to 67.7%, respectively (SI Tables S1−S3). The extractable organic matter (such as bitumen and tar) showed little effect on chemical composition of Z-BCs at above 400 °C (SI Table S1). As the pyrolysis temperature increased, the values of O% (17.6−28.1%, 16.6−26.7%), H% (4.16−6.05%, 3.59−5.24%), H/C (0.69−1.06, 0.66−1.00), O/C (0.18−0.30, 0.19−0.30), and (N+O)/C (0.21−0.32, 0.22−0.32) for ZHP-BCs and ZSH-BCs decreased at first and then increased, reaching the lowest values at 350 or 400 °C (SI Table S2). Moreover, the ZSH-BCs had lower OC contents, H contents, and H/C values than did the ZHP-BCs, indicating that NaClO oxidized more organic matter than H_2O_2 did.

For the PHP-BCs and PSH-BCs, the OC contents were in the ranges of 66.5−75.7% and 61.5−69.2%, respectively (SI Table S3). As the pyrolysis temperature increased, the variation trends of O% (13.7−21.6%, 12.9−20.2%), O/C

DOI: 10.1021/acs.est.9b01788
Environ. Sci. Technol. 2019, 53, 7683−7693

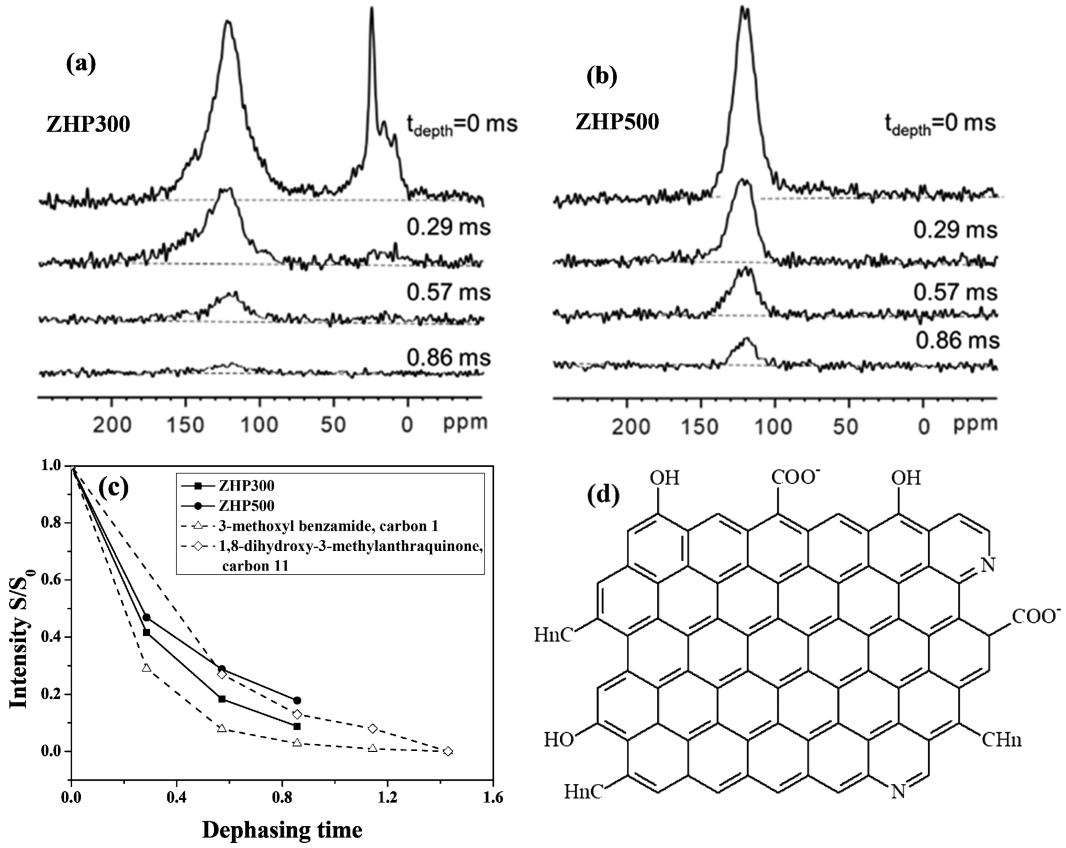

Figure 2. Series of ^{13}C DP/TOSS spectra after $^{1}H-^{13}C$ recoupled long-range dipolar dephasing at the indicated durations t_{deph} on ZHP300 (a) and ZHP500 (b). (c) Plot of the signal areas of aromatic carbons resonating between 107 and 142 ppm versus dephasing time. Solid circles: ZHP300. Solid squares: ZHP500. Open triangles: Carbon 1 of 3-methoxylbenzamide, which is two bonds away from the two nearest protons. Open diamonds: Carbon 11 of 1,8-dihydroxy-3-methylanthraquinone, which is three bonds away from the three nearest protons. (d) Model of aromatic cluster for ZHP500, derived from NMR spectroscopy and H−C distance measurements.

(0.14−0.24, 0.14−0.25), and (N+O)/C (0.17−0.27, 0.17−0.27) for PHP-BCs and PSH-BCs were consistent with those of ZHP-BCs and ZSH-BCs, whereas the H contents (3.22−6.40%, 2.84−6.17%) and H/C values (0.54−1.16, 0.50−1.17) for PHP-BCs and PSH-BCs gradually decreased (SI Table S3). Similarly, the PSH-BCs exhibited lower OC, O, and H contents than the PHP-BCs. The differences in the elemental contents of the different BCs may be due to the diverse activation mechanisms of $ZnCl_2$ and KOH. That is, $ZnCl_2$ activation mainly caused dehydration, whereas KOH reacted with C atoms.[13,16] Moreover, the activated and oxidized BCs in the current research gave higher O/C (0.14−0.30) values than the inactivated kerogen-derived BCs (O/C, 0.046−0.14),[10,11] demonstrating that activation and oxidization lowered the hydrophobicity of these BCs.

Surface Properties and Chemical Structures of BCs. For ZHP-BCs and ZSH-BCs, the total surface acidic functional groups (3.35−7.24 mmol/g) were reduced gradually, whereas the basic functional groups (1.03−1.61 mmol/g) fluctuated slightly with increasing pyrolysis temperature (SI Table S2). The total surface acidic functional groups (4.07−7.84 mmol/g) of PHP-BCs and PSH-BCs were higher than those of ZPH-BCs and ZSH-BCs, whereas the reverse trend was true for those of basic functional groups (0.02−1.33 mmol/g) (SI Table S3). In addition, the total acidic functional groups of PHP-BCs and PSH-BCs decreased at first and then elevated with increasing pyrolysis temperature and reached the lowest values at 350 or 400 °C. Our activated and oxidized BCs demonstrated lower total surface acidic groups (3.35−7.84 mmol/g) than did the biomass-derived BCs produced at temperatures ranging from 250 to 600 °C (4.4−8.1 mmol/g).[43] Moreover, the activated and oxidized BCs in the present study gave higher CEC values (36.2−222 cmol/kg, SI Tables S2 and S3) than did the biomass-derived or poultry litter-derived BCs (1.3−94.2 cmol/kg).[42−46] Lehmann et al.[45] and Liang et al.[47] showed that the addition of oxidized black carbon to the soil increased the CEC values of the soil and had better agricultural applications. Generally, the CEC values of all the samples were elevated with increasing pyrolysis temperature, which was consistent with those of the wheat straw-derived BCs.[48] The CEC values of NaClO-oxidized BCs were lower than those of H_2O_2-oxidized BCs. Furthermore, the CEC values of the $ZnCl_2$-activated BCs were higher than those of KOH-activated BCs, suggesting that $ZnCl_2$ could better enhance the CEC values of the samples.

Generally speaking, the water contact angles for our BCs decreased with the increasing temperature (SI Tables S1−S3), indicating the enhanced hydrophilicity of BCs. If the water contact angle is >90°, the BC surface is hydrophobic. BCs produced at high temperature (≥400 or 450 °C) become hydrophilic in this investigation, which is consistent with other investigation.[35] Suliman et al. reported that pine wood-derived biochar produced at 600 °C were much more hydrophilic than that produced at 350 °C.[35]

Figure 1 was the multiCP/MAS spectra of BCs. Except for OS, the aromatic carbon (F_{aro}%) (34.8−94.8%) in all the

DOI: 10.1021/acs.est.9b01788
Environ. Sci. Technol. 2019, 53, 7683−7693

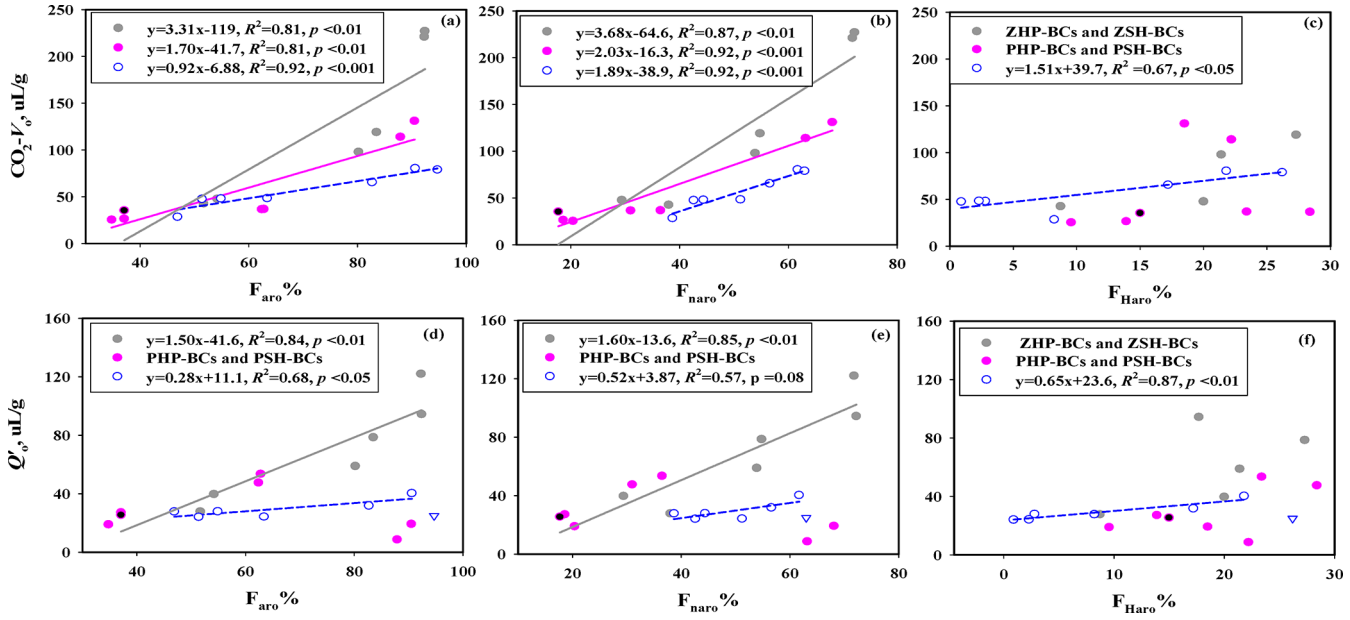

Figure 3. Relationships of the micropore volumes CO_2-V_0 and adsorption volumes Q_0' of phenanthrene with F_{aro}%, F_{naro}%, and F_{Haro}% on the BCs. In the graph, the gray lines represent the ZHP-BCs and ZSH-BCs, the pink lines represent the PHP-BCs and PSH-BCs, and the blue lines represent the inactivated kerogen-derived BCs. The outlier of inactivated kerogen-derived BC at 500 °C is shown in the blank triangle mark and not included in the corresponding correlation equation. The black dots are OS and are included in the correlation equation.

samples, especially that of nonprotonated aromatic carbon (F_{naro}%) (18.6−74.8%), increased with an increase in the pyrolysis temperature, while protonated aromatic carbon (F_{Haro}%) (8.73−28.4%) decreased drastically at 500 °C (SI Table S4). The elevated nonprotonated aromatic carbon fractions suggested that the heat treatment induced a high degree of aromatic condensation, which may also result in larger aromatic cluster sizes.[12] In addition, F_{aro}% values of BCs (34.8−94.8%) in the present research were slightly lower than those of inactivated kerogen-derived BCs in another report (54.9−94.7%).[11] In general, BCs, which were produced at relatively low temperatures (<500 °C), consisted mainly of small clusters of condensed carbon, and lacked a high proportion of bridgehead carbon.[38] However, at 500 °C, except for PSH500, the aromatic cluster sizes (58−96) of the investigated BCs were larger than those of inactivated kerogen-derived BCs (38),[11] NaOH-activated biochar (27),[12] and wood-derived char (40) produced at 500 °C,[38] as well as biomass-derived biochar (37−76) produced at 600 or 700 °C.[38,45] The difference in the aromatic cluster sizes between previous reports and our present work may be the effects of $ZnCl_2$ or KOH,[11,38] as the activating agents can promote the carbonization and aromatization of the carbon skeleton and result in larger aromatic cluster sizes at a relatively high temperature (500 °C).[16] For different activating agents, $ZnCl_2$-activated and oxidized BCs had a higher F_{aro}% (51.7−92.4%) and F_{naro}% (29.4−72.2%) than the KOH-activated and oxidized BCs (34.8−90.5% and 18.6−68.1%, respectively), whereas F_{Haro}% did not (except for ZHP300). Another report has also shown that $ZnCl_2$-activated carbon exhibited more aromatic carbon contents than did KOH-activated carbon.[49] For the two different oxidizing agents, the NaClO-oxidized BCs provided higher alkoxy carbon (F_{Oalk}%, 2.26−4.44%) and lower F_{aro}% (34.8−92.3%) than did H_2O_2-oxidized BCs (2.39−3.75% and 37.1−92.4%, respectively).

Due to the strong distance dependence of $^1H-^{13}C$ dipolar couplings, the size of clusters of fused aromatic rings in these BCs were estimated by $^1H-^{13}C$ long-range dipolar dephasing (Figure 2a,b).[39] The dephasing rate of the ZHP300 nearly coincided with that of the two-bond model, indicating that the carbons in this char were on average at a two-bond distance from the nearest proton (Figure 2c). The ZHP500 had a slower dephasing rate compared to the ZHP300, and its dephasing curve was similar to that of the three-bond calibration curve, consistent with the 500 °C char produced by wood.[38] Based on the NMR composition and H−C distance data, a structural model for a typical aromatic ring of the ZHP500 can be proposed (Figure 2d). The structure contained 29 rings and 76 aromatic carbons, with an average H−C distance of 2.97 bond, which is consistent with the three-bond calibration curve.

Micropore, Mesopore, and Micropore Size Distributions. The CO_2-V_0 (37.2−258 μL/g) and CO_2−SSA (92.8−644 m^2/g) of the Z-BCs, E-Z-BCs, ZHP-BCs, and ZSH-BCs increased with increasing pyrolysis temperature (SI Tables S5 and S6). The extractable organic matter (such as bitumen and tar) showed little effect on micropore and mesopore volumes of Z-BCs at above 400 °C. Moreover, the CO_2-V_0 (23.6−131 μL/g) and CO_2−SSA (58.9−328 m^2/g) of PHP-BCs and PSH-BCs decreased at first and then increased with increasing pyrolysis temperature and were much lower than those of ZHP-BCs and ZSH-BCs (SI Table S6). Our previous investigation showed that the CO_2-V_0 and CO_2−SSA values of inactivated kerogen-derived BCs were 47.6−80.4 μL/g and 114−192 m^2/g, respectively.[11] The $ZnCl_2$ activation and oxidation treatments elevated their CO_2-V_0 and CO_2−SSA values by 24.6−188% and 29.3−200%, respectively, at above 300 °C. The KOH activation and oxidation treatments enhanced their CO_2-V_0 and CO_2−SSA values by 20.6−66.0% and 26.6−73.5%, respectively, at above 400 °C. In the present study, in the low temperature stage (<300 or 400 °C), the values of CO_2-V_0 and CO_2−SSA are lower than those of inactivated kerogen-derived BCs. This phenomenon may be related to the fact that the activation agents could not react

DOI: 10.1021/acs.est.9b01788
Environ. Sci. Technol. 2019, 53, 7683−7693

Table 1. Sorption and Desorption Model Parameters, *K*oc Values, and Hysteresis Indices for the Extracted $ZnCl_2$-Activated BCs

						logKoc,mL/g			HI[c]		
sample	logK_F[a]	n	N[b]	R^2	foc(%)	$C_e = 0.01S_w$	$C_e = 0.1S_w$	$C_e=S_w$	$C_e = 0.01S_w$	$C_e = 0.1S_w$	$C_e=S_w$
E-Z250-S	2.84 ± 0.049[d]	0.656 ± 0.012[e]	12	0.975	66.9	5.65	5.31	4.97	0.553	0.570	0.588
E-Z250-D	3.02 ± 0.019	0.668 ± 0.011	14	0.985	66.9	5.85	5.52	5.18			
E-Z300-S	3.00 ± 0.013	0.688 ± 0.018	13	0.982	69.1	5.83	5.52	5.21	1.19	0.690	0.303
E-Z300-D	3.48 ± 0.028	0.566 ± 0.027	14	0.993	69.1	6.19	5.75	5.32			
E-Z350-S	3.64 ± 0.011	0.526 ± 0.005	14	0.996	71.6	6.29	5.82	5.34	0.431	0.327	0.231
E-Z350-D	3.83 ± 0.006	0.493 ± 0.001	14	0.996	71.6	6.45	5.94	5.43			
E-Z400-S	3.83 ± 0.038	0.492 ± 0.019	13	0.989	73.8	6.43	5.92	5.41	0.365	0.274	0.190
E-Z400-D	3.96 ± 0.011	0.481 ± 0.007	12	0.994	73.8	6.55	6.03	5.51			
E-Z450-S	3.92 ± 0.025	0.505 ± 0.013	13	0.991	74.3	6.53	6.03	5.54	0.323	0.123	
E-Z450-D	4.08 ± 0.012	0.449 ± 0.008	14	0.994	74.3	6.63	6.08	5.53			
E-Z500-S	4.12 ± 0.029	0.487 ± 0.010	14	0.992	74.8	6.70	6.19	5.68	0.110		
E-Z500-D	4.21 ± 0.022	0.438 ± 0.013	14	0.990	74.8	6.75	6.19	5.63			

[a]logK_F is the sorption affinity coefficient with units of $(\mu g/g)/(\mu g/L)^n$. [b]Number of data. [c]HI is hysteresis index, HI= $\frac{q_e^d - q_e^s}{q_e^s}|_{T,C_e}$ [d]Standard deviation of logK_F. [e]Standard deviation of n.

Table 2. Freundlich Isotherm Parameters of Phenanthrene for the $ZnCl_2$- or KOH-Activated and Oxidized BCs

					logKOC,mL/g		
sample	logK_F[a]	n	N[b]	R^2	$C_e = 0.01S_w$	$C_e = 0.1S_w$	$C_e=S_w$
OS	2.45 ± 0.027[c]	0.729 ± 0.004[d]	18	0.996	5.33	5.06	4.79
ZHP250	2.48 ± 0.015	0.692 ± 0.006	18	0.997	5.32	5.01	4.71
ZHP300	2.90 ± 0.040	0.639 ± 0.016	19	0.998	5.67	5.31	4.95
ZHP350	3.22 ± 0.022	0.585 ± 0.007	20	0.997	5.92	5.51	5.09
ZHP400	3.61 ± 0.034	0.501 ± 0.014	19	0.996	6.23	5.73	5.23
ZHP450	3.81 ± 0.035	0.444 ± 0.009	19	0.986	6.37	5.82	5.26
ZHP500	3.97 ± 0.009	0.419 ± 0.004	19	0.992	6.52	5.94	5.35
ZSH250	2.33 ± 0.021	0.780 ± 0.009	18	0.993	5.30	5.08	4.86
ZSH300	2.43 ± 0.025	0.757 ± 0.017	20	0.994	5.36	5.12	4.88
ZSH350	2.82 ± 0.012	0.663 ± 0.002	19	0.993	5.64	5.31	4.97
ZSH400	2.93 ± 0.036	0.696 ± 0.017	19	0.992	5.80	5.50	5.19
ZSH450	3.55 ± 0.022	0.538 ± 0.021	19	0.993	6.25	5.78	5.32
ZSH500	3.85 ± 0.004	0.471 ± 0.011	19	0.991	6.46	5.93	5.41
PHP250	1.78 ± 0.005	0.934 ± 0.002	17	0.989	4.89	4.83	4.76
PHP300	1.97 ± 0.000	0.912 ± 0.001	18	0.993	5.04	4.95	4.87
PHP350	2.02 ± 0.039	0.937 ± 0.020	17	0.990	5.09	5.03	4.96
PHP400	3.03 ± 0.061	0.612 ± 0.026	18	0.985	5.75	5.36	4.97
PHP450	2.98 ± 0.049	0.609 ± 0.025	17	0.991	5.73	5.34	4.94
PHP500	2.97 ± 0.029	0.525 ± 0.018	16	0.981	5.62	5.14	4.67
PSH250	2.16 ± 0.042	0.725 ± 0.013	18	0.984	5.08	4.81	4.53
PSH300	2.30 ± 0.022	0.733 ± 0.014	18	0.990	5.22	4.95	4.68
PSH350	2.57 ± 0.005	0.748 ± 0.010	20	0.994	5.48	5.23	4.98
PSH400	3.22 ± 0.002	0.580 ± 0.005	18	0.991	5.94	5.52	5.10
PSH450	2.94 ± 0.008	0.546 ± 0.003	19	0.983	5.63	5.18	4.72
PSH500	2.49 ± 0.035	0.486 ± 0.039	18	0.976	5.12	4.61	4.09

[a]logK_F is the sorption affinity coefficient with units of $(\mu g/g)/(\mu g/L)^n$. [b]Number of data. [c]Standard deviation of logK_F. [d]Standard deviation of n.

adequately to produce micropore, at temperature below their melting points. The melting points of $ZnCl_2$ and KOH were reported to be 290 and 409 °C, respectively.[49] Furthermore, except for ZSH450 and PSH350, the CO_2-V_0 and CO_2−SSA values of NaClO-oxidized BCs were lower than those of H_2O_2-oxidized BCs, which is consistent with one of our reports.[8] The CO_2-V_0 values of the $ZnCl_2$- and KOH-activated and oxidized BCs were significantly positively correlated with the aromatic carbon (F_{aro}%) and the nonprotonated aromatic carbon (F_{naro}%) of the BCs (Figure 3), suggesting that the nonprotonated aromatic carbon is the main structure responsible for the production of micropore with the activation treatments in the current work, which is consist with the result of the inactivated kerogen-derived BCs.[11]

For N_2 adsorption at the low temperature stages (<400 °C), the micropore (N_2-V_{micro}) and mesopore volumes (N_2-V_{meso}) of Z-BCs, E-Z-BCs, ZHP-BCs, and ZSH-BCs were very low and can be ignored. However, at above 400 °C, the N_2-V_{micro} and N_2-V_{meso} of Z-BCs, E-Z-BCs, ZHP-BCs, and ZSH-BCs ranged from 188−384 μL/g and 34.0−80.0 μL/g, respectively. Moreover, at above 400 °C, the adsorption isotherms of $ZnCl_2$ activated BCs were type I isotherms, and were different from

DOI: 10.1021/acs.est.9b01788
Environ. Sci. Technol. 2019, 53, 7683−7693

the type III isotherms of other BCs (SI Figure S3). The N_2-V_{micro} and N_2-V_{meso} for PHP-BCs and PSH-BCs were in the range of 0.07−5.02 μL/g and 0.37−19.7 μL/g, respectively, and were much lower than their CO_2-V_0. As N_2-V_{micro} and N_2-V_{meso} values were very low or even not measured for some BCs, we only discussed the micropore volumes derived from the CO_2 adsorption in the following discussion.

The micropore sizes for all the BCs were mainly concentrated at 0.4−0.9 nm (SI Figure S2). However, the percentages of micropore sizes concentrated at >1.1 nm for the Z-BCs, E-Z-BCs, ZHP-BCs, and ZSH-BCs decreased slightly with increasing pyrolysis temperature and were obviously enhanced at 450 and 500 °C. The micropore sizes of the $ZnCl_2$-activated BCs became larger at higher temperatures (SI Tables S5 and S6). For the PHP-BCs and PSH-BCs, the micropores were mainly concentrated at >1.1 nm at temperatures lower than 400 °C. However, when the temperatures were greater than 400 °C, the micropores for the PHP-BCs and PSH-BCs were mainly concentrated at 0.37−0.7 nm, and their proportions can reach 66.1%, demonstrating that the micropore sizes of the KOH-activated BCs decreased significantly at higher temperatures. The above results showed that under the condition of the present study, the $ZnCl_2$-activated BCs exhibited higher micropore volumes and larger micropore sizes than the KOH-activated BCs did.

Sorption Isotherms of Phenanthrene on BCs. The FM satisfactorily described all the sorption data of phenanthrene with R^2 ranging from 0.975 to 0.998. The isotherm nonlinearity factor n values ranging from 0.419 to 0.937 (Table 1 and Table 2). Generally, the n values of phenanthrene on the BCs decreased with increasing pyrolysis temperature. In addition, the n values of these activated and oxidized BC_S in the present study (0.419−0.937) were higher than those of the inactivated kerogen-derived BCs (0.399−0.753).[10,11] The presence of activating and oxidation agents could change the structure of kerogen,[18] which retards the interlayer space decreasing, and thus, leads to similar or slightly weaker nonlinear sorption on the investigative BCs in comparison with that on the inactivated kerogen-derived BCs (SI Figure S12). For different activation agents, the n values of $ZnCl_2$-activated BCs (0.419−0.780) were lower than those of KOH-activated BCs (0.486−0.937). Moreover, the n values of the PHP-BCs and PSH-BCs were positively correlated with H/C, consistent with the results of inactivated kerogen-derived BCs and our previous modified black carbons.[8,11] Nevertheless, the n values of the ZHP-BCs and ZSH-BCs had no significant relationship with H/C (SI Figure S6). Specifically, there were significant negative correlations of the n values with the aromatic carbon (F_{aro}%), nonprotonated carbon (F_{naro}%) (SI Figure S12) and micropore volumes V_0-CO_2 (SI Figure S6). The results revealed that with increasing temperature, the larger aromaticity and micropore volumes resulted in stronger nonlinear sorption, consistent with other investigations.[10,11]

The sorption affinities log K_{OC}(mL/g) at $C_e = 0.01S_w$ of the ZHP-BCs and ZSH-BCs ranged from 5.30 to 6.52 and were greater than those of the PHP-BCs and PSH-BCs (4.89−5.94), but were lower than those of the E-Z-BCs (5.65−6.70). The log K_{OC} values of the E-Z-BCs, ZHP-BCs, and ZSH-BCs increased with increasing pyrolysis temperature, while those of the PHP-BCs and PSH-BCs increased first and then decreased, reaching maximum values at 400 °C. Moreover, the log K_{OC} values of the E-Z-BCs, ZHP-BCs, and ZSH-BCs (except for ZHP250, ZSH250, and ZSH300) were greater than those of the inactivated kerogen-derived BCs (5.64−6.20 mL/g),[10,11] indicating that the E-Z-BCs, ZHP-BCs, and ZSH-BCs enhanced the sorption affinities of phenanthrene due to the higher micropore volumes. However, the log K_{OC} values of the PHP-BCs and PSH-BCs (4.89−5.94 mL/g) were much lower than those of the inactivated kerogen-derived BCs (5.64−6.20 mL/g),[10] especially of the BCs at 450 and 500 °C. The lower log K_{OC} values of PHP-BCs and PSH-BCs may be due to the following reasons. First, when the pyrolysis temperatures were lower than 400 °C, the micropore volumes of the investigated BCs were lower than those of the inactivated kerogen BCs, which were responsible for the low sorption affinities. Second, when the pyrolysis temperatures were higher than 400 °C, PHP-BCs and PSH-BCs had high micropore volumes, but a considerable portion of these pores was mainly concentrated at 0.37−1.1 nm micropore sizes and were inaccessible by phenanthrene, as phenanthrene is a large-sized molecules (0.341 × 0.999 × 1.094 nm).[8,11] Furthermore, the log K_{OC} (mL/g) values of all the BCs in the present study (4.89−6.70 mL/g) were higher than those of biomass-derived or manure-derived biochar (4.73−5.73 mL/g) produced at temperatures ranging from 300 to 600 °C.[6,50] Compared with other studies, the higher logK_{OC} values in the present work could be explained as follows: On one hand, the CO_2-V_0 values (23.6−258 μL/g) of the BCs in this investigation were larger than those of biomass-derived or manure-derived biochar (9.00−111 μL/g).[50] On the other hand, the presence of activating agents could inhibit the carbon structure contraction,[18] thus resulting in larger micropore spacing, which can be accessible by phenanthrene molecules.

Sorption Irreversibility of Phenanthrene on E-Z-BCs. Desorption hysteresis was quantified by the hysteresis index (HI) according to previously papers.[40,51] If desorption is completely reversible, then HI is equal to 0. The higher is the HI value, the greater the desorption hysteresis is. HI values of E-Z-BCs at $C_e = 0.01S_w$ ranged from 0.11 to 1.19, and increased at first and then decreased with increasing pyrolysis temperature (Table 1). E-Z300 gave the highest HI value, which was likely to be related to micropore deformation mechanism or ink-tank effect.[52] Except for E-Z300, HI values were negatively correlated with CO_2-V_0 (SI Figure S9 (a)) demonstrating that the micropore structure of BCs had a pronounced influence on sorption irreversibility. Similarly, the previous study of our group indicated that sorption irreversibility of benzene on inactivated kerogen-derived BCs was reduced by increasing micropore volumes (SI Table S8 and Figure S9 (b)). Other investigators found that the irreversible sorption induced by either micropore deformation mechanism or ink-tank effect became more pronounced as the pore size decreased.[52] Moreover, E-Z500 in this investigation had the lowest HI value (0.11) and was almost reversible to phenanthrene, suggesting that E-Z500 was fully reversible because it had completely rigid and ordered open pore structures that could not be deformed.

Micropore-Filling Modeling. The *DR* model fits the sorption data well (SI Table S7 and Figure S13) with R^2 values ranging from 0.925 to 0.994. The adsorption volumes Q_0' (20.7−200 μL/g) of the E-Z-BCs, ZHP-BCs, and ZSH-BCs were elevated with the increasing pyrolysis temperature. However, the trends of the adsorption volumes for the PHP-BCs and PSH-BCs (8.71−53.5 μL/g) were enhanced at first and then decreased with increasing pyrolysis temperature. In addition, the adsorption volumes Q_0' (26.2−200 μL/g, except

DOI: 10.1021/acs.est.9b01788
Environ. Sci. Technol. 2019, 53, 7683−7693

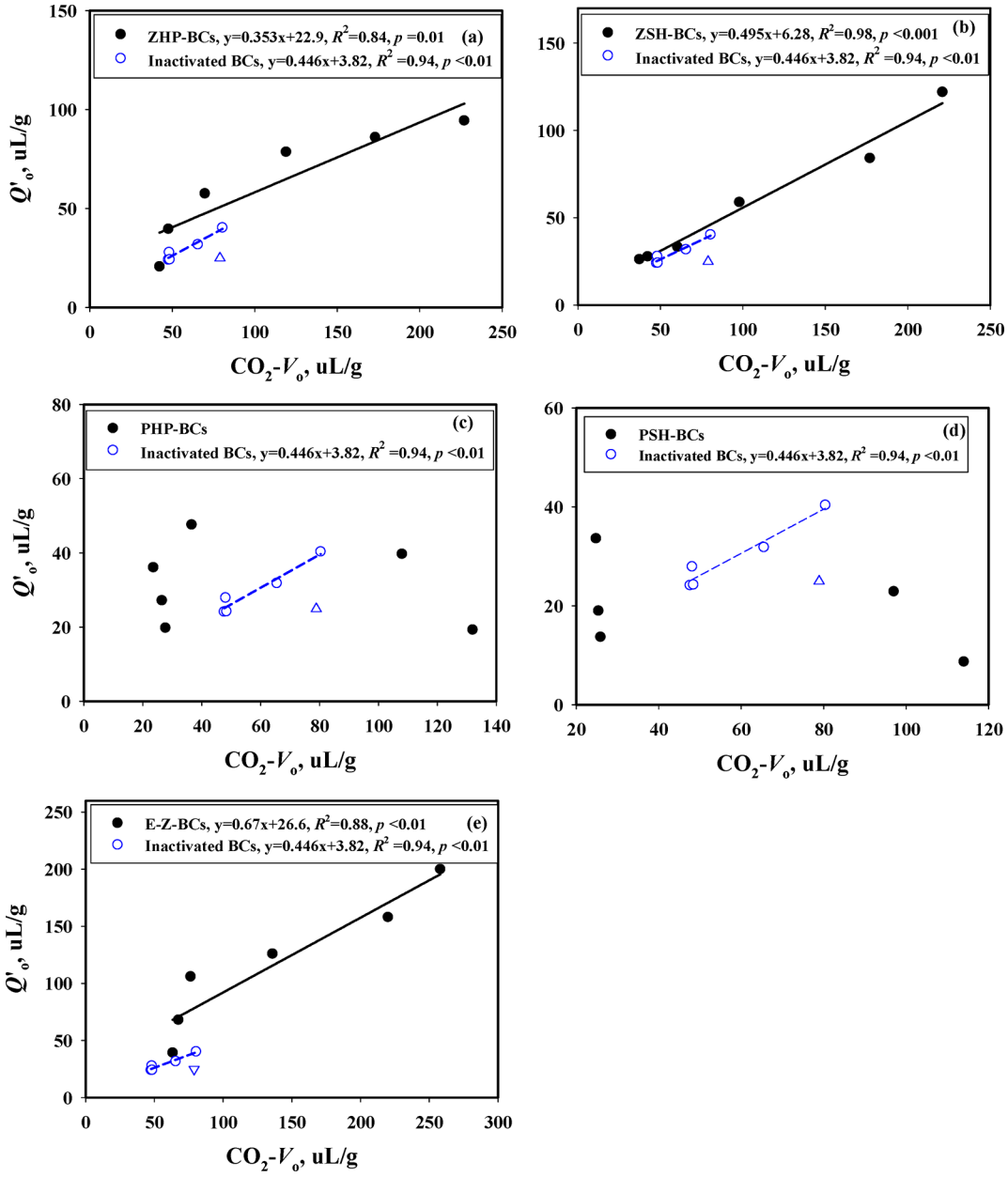

Figure 4. Relationships between the adsorption volumes Q_0' of phenanthrene and the micropore volume (CO_2−V_0) of BCs. In the graph, the black lines are Q_0' calculated by the *DR* model on BCs, and the blue lines are Q_0' calculated by the *DR* model on inactivated kerogen-derived BCs.[11] The outlier of inactivated BC at 500 °C was shown in the blank triangle mark and not included in the corresponding correlation equation.

for ZHP250) of the E-Z-BCs, ZHP-BCs, and ZSH-BCs were larger than those of the inactivated kerogen-derived BCs (24.2−40.4 μL/g, produced at 250−500 °C) or those of biomass or manure-derived BCs (1.03−14.8 μL/g, produced at 450 °C).[10,11,50] Except for E-Z-350, the percentages of Q_0' accounting for CO_2−V_0 on the $ZnCl_2$-activated BCs ranged from 41.6∼101% and were higher than those of the inactivated kerogen-derived BCs (36−65%).[10,11] The results revealed that micropore filling is the main sorption mechanism of phenanthrene on $ZnCl_2$-activated and oxidized BCs. The aromatization of the carbon skeleton by $ZnCl_2$ and the inhibition of carbon structure contraction could contribute to the high micropore volumes and large micropore sizes.[16,18] However, the percentages of Q_0' accounting for CO_2−V_0 for the PHP-BCs and PSH-BCs ranged from 7.64% to 153%. A few of the adsorption volumes were higher than CO_2-V_0, and a few of the adsorption volumes were even less than 10% of CO_2−V_0. The high adsorption percentages were observed for the BCs produced at lower temperatures (<400 °C), whereas the quite low adsorption percentages were found for the BCs produced at higher temperatures (>400 °C). This behavior is likely due to a portion of partitioning sorption in the matrix, which remained in the low-temperature BCs. The decreasing adsorption volumes of KOH-activated BCs were related to the low micropore volumes at lower temperatures (<400 °C) and small micropore sizes at higher temperatures (>400 °C), as the activation of KOH could result in very small micropore sizes.[53]

The Role of Nonprotonated Aromatic Carbon, Micropore Properties, and Surface Properties in Sorption of Phenanthrene on BCs. The log K_{OC} values of the E-Z-BCs, ZHP-BCs, and ZSH-BCs were significantly positively correlated with aromatic carbon (F_{aro}%) or nonprotonated carbon

DOI: 10.1021/acs.est.9b01788
Environ. Sci. Technol. 2019, 53, 7683−7693

(F_{naro}%) (SI Figure S12), and the micropore volume (CO_2−V_0) (SI Figure S10), indicating the effective influences of aromatic carbon and micropore volumes, especially those of micropore volumes at low concentration (C_e = 0.01S_w) on the sorption of HOCs. But for the PHP-BCs and PSH-BCs, the log K_{OC} values were not obviously correlated with aromatic carbon (F_{aro}%), nonprotonated carbon (F_{naro}%), protonated carbon (F_{Haro}%) (SI Figure S12), and the micropore volume (CO_2−V_0) (SI Figure S10). Moreover, the log K_{OC} values of ZHP-BCs, ZSH-BCs, and PSH-BCs were obviously negatively correlated with the surface acidic functional groups (SI Figure S8), while all the BCs showed no relationship with the surface basic groups. In addition, the log K_{OC} values of the ZHP-BCs showed significantly positive correlation with CEC values (SI Figure S8). However, the log K_{OC} values for ZSH-BCs were significantly and positively related to (N+O)/C, but not related to polar carbon (SI Figures S7 and S11). It is noted that the polar carbon is highly related to the thermal pyrolytic temperatures, as demonstrated in SI Table S4 and in previous investigation.[11] The above facts demonstrate that the surface functional groups, polar carbon, and polarity index did not show consistent impact to the sorption of phenanthrene on the BCs, as discussed more in the following paragraph.

The Q'_o values of phenanthrene on the E-Z-BCs, ZHP-BCs, and ZSH-BCs were significantly and positively correlated with the micropore volumes (CO_2−V_0) (Figure 4). It is noted that the R^2 values ranges from 0.84 to 0.98, accounting from the majority of the variability, indicating the dominating effect of micropore-filling volumes in the present study. Compared with the inactivated kerogen-derived BCs, E-Z-BCs, ZHP-BCs, and ZSH-BCs all exhibited much higher micropore volumes and micropore filling volumes. Specially, after the removal of "soft carbon" by oxidization treatments as demonstrated previously,[54] ZSH-BCs showed a nice regression equation between adsorption volumes and micropore volumes (CO_2−V_0), and the equation is Q'_0 = 0.495V_0 + 6.28(R^2 = 0.98, p < 0.001), indicating that the micropore volumes are the dominating factor affecting micropore filling volumes of phenanthrene. However, the Q'_o values showed no relationships with CO_2−V_0 for PHP-BCs and PSH-BCs. But, at above 400 °C, it was found that the DFT−$V_{(0.37-1.1\ nm)}$/DFT−V_0% for PHP-BCs and PSH-BCs were significantly and negatively correlated with adsorption volumes in SI Figure S14, indicating that the important effect of micropore sizes. As phenanthrene molecule is 0.341 × 0.999 × 1.094 nm,[8,11] we divided the micropore size at 1.1 nm. Moreover, recent investigation found that H_2O_2 oxidant can not enter the micropores of resistant organic matter, but can only oxidize desorbed phenanthrene in the solutions.[54] The above results demonstrated that the micropore filling was the dominating adsorption mechanism, and the micropore size distribution affected the adsorption mechanism of phenanthrene.

The obtained modeling results and sorption irreversibility suggest that adsorption (micropore filling) is the dominant sorption mechanism of phenanthrene by the investigated BCs. As demonstrated above, the presence of internal micropore in the BCs is also responsible for the nonlinearity of the phenanthrene sorption isotherms. More importantly, the contents of nonprotonated aromatic carbon, micropore volumes and micropore sizes are the critical factors to micropore filling mechanism of phenanthrene on BCs. The $ZnCl_2$ activation and oxidation treatments are highly efficient, but the KOH activation and oxidation treatments are not as efficient as expected. This finding improves our understanding of the sorption mechanism of hydrophobic organic contaminants (HOCs) from the perspective of chemical structure and micropore, providing a basis for the removal of organic pollutants in the aqueous phase.

■ ASSOCIATED CONTENT

Supporting Information

The Supporting Information is available free of charge on the ACS Publications website at DOI: 10.1021/acs.est.9b01788.

Information on the activated methods, batch sorption and desorption experiments, and sorption models of activated and oxidized BCs. Properties of the elemental composition, surface functional groups, NMR structural parameters, micropore, mesopore, and sorption parameters of activated and oxidized BCs (Tables S1−S7). Sorption and desorption of benzene on inactivated kerogen-derived BCs (Table S8). Sorption isotherms of CO_2, N_2, and micropore size distributions (Figures S1−S3) and sorption isotherms of the FM and *DR* models on the BCs (Figures S4, S5, and S13). Correlation relationships of n with H/C and CO_2-V_0, of log K_{OC} with CEC and surface functional groups, of HI with CO_2-V_0, of log K_{OC} (C_e = 0.01S_w) values with (N+O)/C, CO_2-V_0 and polar carbon, and of the adsorption volumes Q_0' with DFT−$V_{(0.37-1.1\ nm)}$/DFT−V_0% of the activated and oxidized BCs (Figures S6−S12, S14) (PDF)

■ AUTHOR INFORMATION

Corresponding Author

*Phone: 86-20-85290263; fax: 86-20-85290706; e-mail: yran@gig.ac.cn.

ORCID

Yong Ran: 0000-0001-8659-0950

Xiaoyan Cao: 0000-0001-7571-6482

Notes

The authors declare no competing financial interest.

■ ACKNOWLEDGMENTS

This study was supported by a key joint project of the National Natural Science Foundation of China and Guangdong Province, China (U1701244), a project of the National Natural Science Foundation of China (41773137), and a project of the Earmarked Foundation of the State Key Laboratory, China (SKLOG2015A01). We appreciate the Editor and Reviewers for their review time and helpful comments on our manuscript. The ACS ChemWorm is appreciated for the edition of the manuscript. This is contribution no. IS-2714 from GIGCAS.

■ REFERENCES

(1) Cheng, C. H.; Lin, T. P.; Lehmann, J.; Fang, L. J.; Yang, Y. W.; Menyailo, O. V.; Chang, K. H.; Lai, J. S. Sorption properties for black carbon (wood char) after long term exposure in soils. *Org. Geochem.* **2014**, *70*, 53−61.

(2) Guo, X.; Miao, Y.; Yang, C.; Zhang, Q.; Gao, L.; Hu, Y. Sorption of tylosin on black carbon from different sources. *J. Environ. Chem. Eng.* **2016**, *4* (3), 3393−3400.

(3) Xu, X.; Sun, H.; Simpson, M. J. Concentration- and time-dependent sorption and desorption behavior of phenanthrene to

geosorbents with varying organic matter composition. *Chemosphere* **2010**, *79* (8), 772−778.
(4) Qi, F.; Kuppusamy, S.; Naidu, R.; Bolan, N. S.; Ok, Y. S.; Lamb, D.; Li, Y.; Yu, L.; Semple, K. T.; Wang, H. Pyrogenic carbon and its role in contaminant immobilization in soils. *Crit. Rev. Environ. Sci. Technol.* **2017**, *47* (10), 795−876.
(5) Zhang, D.; Duan, D.; Huang, Y.; Yu, Y.; Yong, R. Novel phenanthrene sorption mechanism by two pollens and their fractions. *Environ. Sci. Technol.* **2016**, *50* (14), 7305−7314.
(6) Han, L.; Sun, K.; Jin, J.; Wei, X.; Xia, X.; Wu, F.; Gao, B.; Xing, B. Role of structure and microporosity in phenanthrene sorption by natural and engineered organic matter. *Environ. Sci. Technol.* **2014**, *48* (19), 11227−11234.
(7) Ran, Y.; Xing, B.; Rao, P. S. C.; Fu, J. Importance of adsorption (hole-filling) mechanism for hydrophobic organic contaminants on an aquifer kerogen isolate. *Environ. Sci. Technol.* **2004**, *38* (16), 4340−4348.
(8) Hu, S.; Zhang, D.; Xiong, Y.; Yang, Y.; Ran, Y. Nanopore-filling effect of phenanthrene sorption on modified black carbon. *Sci. Total Environ.* **2018**, *642*, 1050−1059.
(9) Ran, Y.; Yang, Y.; Xing, B.; Pignatello, J. J.; Kwon, S.; Su, W.; Zhou, L. Evidence of micropore filling for sorption of nonpolar organic contaminants by condensed organic matter. *J. Environ. Qual.* **2013**, *42* (3), 806−814.
(10) Zhang, Y.; Ma, X.; Ran, Y. Sorption of phenanthrene and benzene on differently structural kerogen: important role of micropore-filling. *Environ. Pollut.* **2014**, *185*, 213−218.
(11) Duan, D.; Zhang, D.; Ma, X.; Yang, Y.; Ran, Y.; Mao, J. Chemical and structural characterization of thermally simulated kerogen and its relationship with microporosity. *Mar. Pet. Geol.* **2018**, *89*, 4−13.
(12) Park, J.; Hung, I.; Gan, Z.; Rojas, O. J.; Lim, K. H.; Park, S. Activated carbon from biochar: Influence of its physicochemical properties on the sorption characteristics of phenanthrene. *Bioresour. Technol.* **2013**, *149*, 383−389.
(13) Wang, J.; Kaskel, S. KOH activation of carbon-based materials for energy storage. *J. Mater. Chem.* **2012**, *22* (45), 23710−23725.
(14) Yang, J.; Qiu, K. Preparation of activated carbons from walnut shells via vacuum chemical activation and their application for methylene blue removal. *Chem. Eng. J.* **2010**, *165* (1), 209−217.
(15) Mohanty, K.; Das, D.; Biswas, M. Adsorption of phenol from aqueous solutions using activated carbons prepared from Tectona-grandis sawdust by $ZnCl_2$ activation. *Chem. Eng. J.* **2005**, *115* (1), 121−131.
(16) Olivares-Marín, M.; Fernández-González, C.; Macías-García, A.; Gómez-Serrano, V. Preparation of activated carbon from cherry stones by chemical activation with $ZnCl_2$. *Appl. Surf. Sci.* **2006**, *252* (17), 5967−5971.
(17) Armandi, M.; Bonelli, B.; Geobaldo, F.; Garrone, E. Nanoporous carbon materials obtained by sucrose carbonization in the presence of KOH. *Microporous Mesoporous Mater.* **2010**, *132* (3), 414−420.
(18) Molina-Sabio, M.; Rodrı′guez-Reinoso, F. Role of chemical activation in the development of carbon porosity. *Colloids Surf., A* **2004**, *241* (1−3), 15−25.
(19) Regmi, P.; Garcia Moscoso, J. L.; Kumar, S.; Cao, X.; Mao, J.; Schafran, G. Removal of copper and cadmium from aqueous solution using switchgrass biochar produced via hydrothermal carbonization process. *J. Environ. Manage.* **2012**, *109*, 61−69.
(20) Ahmadpour, A.; Do, D. The preparation of active carbons from coal by chemical and physical activation. *Carbon* **1996**, *34* (4), 471−479.
(21) Radhika, M.; Palanivelu, K. Adsorptive removal of chlorophenols from aqueous solution by low cost adsorbent - Kinetics and isotherm analysis. *J. Hazard. Mater.* **2006**, *138* (1), 116−124.
(22) Yahya, M. A.; Al-Qodah, Z.; Ngah, C. W. Z. Agricultural bio-waste materials as potential sustainable precursors used for activated carbon production: A review. *Renewable Sustainable Energy Rev.* **2015**, *46*, 218−235.
(23) Ran, Y.; Sun, K.; Yang, Y.; Xing, B.; Zeng, E. Strong sorption of phenanthrene by condensed organic matter in soils and sediments. *Environ. Sci. Technol.* **2007**, *41* (11), 3952−3958.
(24) Yang, J.; Qiu, K. Q. Preparation of activated carbon by chemical activation under vacuum. *Environ. Sci. Technol.* **2009**, *43* (9), 3385.
(25) Oliveira, L. C.; Pereira, E.; Guimaraes, I. R.; Vallone, A.; Pereira, M.; Mesquita, J. P.; Sapag, K. Preparation of activated carbons from coffee husks utilizing $FeCl_3$ and $ZnCl_2$ as activating agents. *J. Hazard. Mater.* **2009**, *165* (1), 87−94.
(26) Ahmadpour, A.; Do, D. The preparation of activated carbon from macadamia nutshell by chemical activation. *Carbon* **1997**, *35* (12), 1723−1732.
(27) Lillo-Ródenas, M. A.; Ros, A.; Fuente, E.; Montes-Morán, M. A.; Martin, M. J.; Linares-Solano, A. Further insights into the activation process of sewage sludge-based precursors by alkaline hydroxides. *Chem. Eng. J.* **2008**, *142* (2), 168−174.
(28) Dıaz-Terán, J.; Nevskaia, D.; Fierro, J.; López-Peinado, A.; Jerez, A. Study of chemical activation process of a lignocellulosic material with KOH by XPS and XRD. *Microporous Mesoporous Mater.* **2003**, *60* (1), 173−181.
(29) Lozano-Castello, D.; Calo, J.; Cazorla-Amoros, D.; Linares-Solano, A. Carbon activation with KOH as explored by temperature programmed techniques, and the effects of hydrogen. *Carbon* **2007**, *45* (13), 2529−2536.
(30) Paul, S.; Veldkamp, E.; Flessa, H. Differential response of mineral-associated organic matter in tropical soils formed in volcanic ashes and marine Tertiary sediment to treatment with HCl, NaOCl, and $Na_4P_2O_7$. *Soil Biol. Biochem.* **2008**, *40* (7), 1846−1855.
(31) Siregar, A.; Kleber, M.; Mikutta, R.; Jahn, R. Sodium hypochlorite oxidation reduces soil organic matter concentrations without affecting inorganic soil constituents. *Eur. J. Soil Sci.* **2005**, *56* (4), 481−490.
(32) Boehm, H. Some aspects of the surface chemistry of carbon blacks and other carbons. *Carbon* **1994**, *32* (5), 759−769.
(33) Chun, Y.; Sheng, G.; Chiou, C. T.; Xing, B. Compositions and sorptive properties of crop residue-derived chars. *Environ. Sci. Technol.* **2004**, *38* (17), 4649−4655.
(34) Zhang, W.; Wang, L.; Sun, H. Modifications of black carbons and their influence on pyrene sorption. *Chemosphere* **2011**, *85* (8), 1306−1311.
(35) Suliman, W.; Harsh, J. B.; Abu-Lail, N. I.; Fortuna, A.; Dallmeyer, I.; Garcia-Pérez, M. The role of biochar porosity and surface functionality in augmenting hydrologic properties of a sandy soil. *Sci. Total Environ.* **2017**, *574*, 139−147.
(36) Johnson, R. L.; Schmidt-Rohr, K. Quantitative solid-state ^{13}C NMR with signal enhancement by multiple cross polarization. *J. Magn. Reson.* **2014**, *239*, 44−49.
(37) Mao, J.; Fang, X.; Lan, Y.; Schimmelmann, A.; Mastalerz, M.; Xu, L.; Schmidt-Rohr, K. Chemical and nanometer-scale structure of kerogen and its change during thermal maturation investigated by advanced solid-state ^{13}C NMR spectroscopy. *Geochim. Cosmochim. Acta* **2010**, *74* (7), 2110−2127.
(38) Cao, X.; Pignatello, J. J.; Li, Y.; Lattao, C.; Chappell, M. A.; Chen, N.; Miller, L. F.; Mao, J. Characterization of wood chars produced at different temperatures using advanced solid-state ^{13}C NMR spectroscopic techniques. *Energy Fuels* **2012**, *26* (9), 5983−5991.
(39) Mao, J. D.; Schmidt-Rohr, K. Recoupled long-range C−H dipolar dephasing in solid-state NMR, and its use for spectral selection of fused aromatic rings. *J. Magn. Reson.* **2003**, *162*, 217−227.
(40) Huang, W.; Weber, W. J., Jr. A distributed reactivity model for sorption by soils and sediments. 10. Relationships between desorption, hysteresis, and the chemical characteristics of organic domains. *Environ. Sci. Technol.* **1997**, *31*, 2562−2569.
(41) Ran, Y.; Huang, W.; Rao, P. S. C.; Liu, D.; Sheng, G.; Fu, J. The role of condensed organic matter in the nonlinear sorption of hydrophobic organic contaminants by a peat and sediments. *J. Environ. Qual.* **2002**, *31*, 1953−1962.

DOI: 10.1021/acs.est.9b01788
Environ. Sci. Technol. 2019, 53, 7683−7693

(42) Kleineidam, S.; Schüth, C.; Grathwohl, P. Solubility-normalized combined adsorption-partitioning sorption isotherms for organic pollutants. *Environ. Sci. Technol.* **2002**, *36* (21), 4689−4697.
(43) Mukherjee, A.; Zimmerman, A. R.; Harris, W. Surface chemistry variations among a series of laboratory-produced biochars. *Geoderma* **2011**, *163* (3−4), 247−255.
(44) Wang, Y.; Hu, Y.; Zhao, X.; Wang, S.; Xing, G. Comparisons of biochar properties from wood material and crop residues at different temperatures and residence times. *Energy Fuels* **2013**, *27* (10), 5890−5899.
(45) Lehmann, J.; Rillig, M. C.; Thies, J.; Masiello, C. A.; Hockaday, W. C.; Crowley, D. Biochar effects on soil biota − A review. *Soil Biol. Biochem.* **2011**, *43* (9), 1812−1836.
(46) Nguyen, B. T.; Lehmann, J. Black carbon decomposition under varying water regimes. *Org. Geochem.* **2009**, *40* (8), 846−853.
(47) Liang, B.; Lehmann, J.; Solomon, D.; Kinyangi, J.; Grossman, J.; O'Neill, B.; Skjemstad, J. O.; Thies, J.; Luizão, F. J.; Petersen, J. Black carbon increases cation exchange capacity in soil. *Soil Sci. Soc. Am. J.* **2006**, *70* (5), 1719−1730.
(48) Zhao, L.; Cao, X.; Mašek, O.; Zimmerman, A. Heterogeneity of biochar properties as a function of feedstock sources and production temperatures. *J. Hazard. Mater.* **2013**, *256*−*257*, 1−9.
(49) Ma, Y. Comparison of activated carbons prepared from wheat straw via $ZnCl_2$ and KOH activation. *Waste Biomass Valorization* **2017**, *8* (3), 549−559.
(50) Jin, J.; Sun, K.; Yang, Y.; Wang, Z.; Han, L.; Wang, X.; Wu, F.; Xing, B. Comparison between soil- and biochar-derived humic acids: composition, conformation, and phenanthrene sorption. *Environ. Sci. Technol.* **2018**, *52* (4), 1880−1888.
(51) Liu, J.; Ma, Y.; Zhu, D.; Xia, T.; Qi, Y.; Yao, Y.; Guo, X.; Ji, R.; Chen, W. Polystyrene nanoplastics-enhanced contaminant transport: role of irreversible adsorption in glassy polymeric domain. *Environ. Sci. Technol.* **2018**, *52*, 2677−2685.
(52) Wang, B.; Zhang, W.; Li, H.; Fu, H.; Qu, X.; Zhu, D. Micropore clogging by leachable pyrogenic organic carbon: a new perspective on sorption irreversibility and kinetics of hydrophobic organic contaminants to black carbon. *Environ. Pollut.* **2017**, *220*, 1349−1358.
(53) Fu, Y.; Zhang, N.; Shen, Y.; Ge, X.; Chen, M. Micro-mesoporous carbons from original and pelletized rice husk via one-step catalytic pyrolysis. *Bioresour. Technol.* **2018**, *269*, 67−73.
(54) Zhuo, C.; Zhang, D.; Yang, Y.; Ran, Y.; Zhang, X.; Mao, J. Effects of compositions, chemical structures, and microporosity of sedimentary organic matter on degradation of benzo(a)pyrene by hydrogen peroxide. *Water Res.* **2019**, *159*, 414.

DOI: 10.1021/acs.est.9b01788
Environ. Sci. Technol. 2019, 53, 7683−7693